Off-axis response and shear characterization of unidirectional ply-level hybrid carbon-fiber-reinforced polymer materials

Maria CASAPU*[,1,2,3], Michel ARRIGONI[2], Ion FUIOREA[1,3]

*Corresponding author
[1]University POLITEHNICA of Bucharest,
313 Splaiul Independentei, Sector 6, 060042 Bucharest, Romania,
maria.demsa@mta.ro*
[2]ENSTA Bretagne, IRDL, UMR CNRS 6027,
2 rue François VERNY, 29806 Brest Cedex 09, France
[3]Military Technical Academy "Ferdinand I",
39-49 George Cosbuc Avenue, Sector 5, 050141 Bucharest, Romania

DOI: 10.13111/2066-8201.2023.15.3.3

Received: 28 June 2023/ Accepted: 04 July 2023/ Published: September 2023

Abstract: *Composite materials, among them Carbon Fiber Reinforced Polymers (CFRP), have become a key material in structural applications for lightweight structures such as spacecraft and aircraft. CFRP can be found under various quality grades and their mechanical performances increase with their cost and quality grade. In order to limit the costs of the material without degrading technical performances, hybridization could be of interest. However, assessing the conservation of quality standards of hybridized CFRP is crucial. This paper investigates the off-axis mechanical response of ply-level hybrid carbon composites, with varying thickness and material quality. Two types of carbon fiber prepregs were combined in the same laminate using symmetric and asymmetric stacking sequences. Monotonic quasi-static off-axis tests were performed to evaluate the non-linear stress-strain behavior of the laminates, with Digital Image Correlation used to measure strain. The apparent elastic modulus and the in-plane shear modulus were evaluated from the tensile tests at three off-axis angles. The results indicate that the hybrid laminates exhibit higher failure stress levels compared to simple laminates, with an intermediate failure strain. Overall, this study provides insights into the off-axis mechanical behavior of ply-level hybrid carbon fiber composites, with potential applications in the design of composite structures.*

Key Words: *Carbon-fiber, hybridization, off-axis, shear, composites, Digital Image Correlation*

1. INTRODUCTION

Composite materials, particularly Carbon Fiber Reinforced Polymers (CFRP), have emerged as a fundamental material in lightweight structural applications, including spacecraft and aircraft. CFRP is available in different grades, with its mechanical properties improving in tandem with higher cost and quality grades [1]. In order to mitigate costs or reduce the carbon footprint of materials while maintaining technical performance, the concept of hybridization has earned significant attention [2]–[4]. However, it is imperative to evaluate the preservation of quality standards when employing hybridized CFRP materials.

The off-axis tensile test has received significant attention in characterizing the CFRP behavior and verifying the applicability of tensor transformation equations for elastic properties [5], [6]. It provides a convenient approach for estimating in-plane shear properties without requiring specialized fixtures or dedicated composite samples [7]–[10]. Additionally, the test allows for evaluating the strength properties of the composite in different in-plane loading directions, offering valuable insights for design, optimization, and informed decision-making.

Unidirectional (UD) fiber-reinforced composites exhibit anisotropic off-axis mechanical properties due to variations in fiber orientation relative to the loading axis. The axial stress-strain curves of these composites often display non-linear behavior, with the degree of non-linearity influenced by the off-axis angle. Hahn et al. [11] demonstrated the impact of nonlinear constituent laminae on the behavior of laminates through experiments and analytical models. Ogihara et al. [12] investigated the off-axis tensile response of T300/2500 carbon/ epoxy composites, observing apparent softening nonlinearity in the off-axis specimens. Cai et al. [13] examined the off-axis tension behavior of woven glass/epoxy composites and reported a non-linear stress-strain relationship with decreasing elastic moduli as the off-axis angle increased. Ma et al. [14] studied the off-axis behavior of PEEK/AS4 UD thermoplastic composites, finding a linear-elastic relationship during the initial stage and non-linear behavior during the strain-hardening phase.

Various standardized methods exist for characterizing the shear behavior of UD composite materials. ASTM D4255/D4255M [15] and ASTM D5379/D5379M [16], also known as Iosipescu test [17], require specialized fixtures and specific sample shapes ASTM D3518/D3518M [18], involves a ±45° cross-ply laminate that is symmetrically about its midplane. The off-axis tensile test, though lacking standardization, has gained interest for shear properties characterization. Chamis et al [9] studied the 10º off-axis test and recommended it for shear characterization. Pindera et al. [7] conducted a study on seven off-axis configurations and found that shear stress induced by end constraints affects the determination of intralaminar shear modulus G_{12}, necessitating a correction factor for off-axis angles lower than 30º. They concluded that the 45º specimen is ideal for accurately determining G_{12}. In a later study [8], Pindera et al. compared the off-axis test with the Iosipescu test. The 45º off-axis test was recommended for intralaminar shear modulus and the 0º Iosipescu test for shear strength.

DIC has been increasingly used in recent years to measure strain fields during off-axis tensile testing. Merzkirch and Foecke [19] employed DIC strain mapping to analyze the deformation response of CFRP-UD coupon specimens under a 10° off-axis test for shear response analysis. Goidescu et al. [20] conducted an experimental investigation combining full-field measurements, including kinematic (using DIC), thermal, and densimetric measurements, to analyze damage growth in carbon-epoxy laminates subjected to axis and off-axis tensile monotonic tests, and Ma et al. [14] utilized DIC to analyze displacement and strain fields obtained from tests conducted at different off-axis angles. These studies demonstrate the effectiveness of DIC as a robust optical technique for non-contact, full-field measurements.

In our previous work [21], we employed the ply-level hybridization technique and we conducted a preliminary mechanical characterization study of the hybrid and reference materials, examining their density, fiber volume fraction, void content, internal structure, and mechanical response under quasi-static loading in both the fiber and perpendicular directions.

The objectives of this paper are: 1) to complete the mechanical characterization of the UD ply-level hybrid materials; 2) to assess the effects of the hybridization on the off-axis and shear response of carbon fiber UD composite, in comparison to the response of manufactured

reference laminates; 3) to assess the quality of hybridized materials with respect to the reference, in order to validate hybridization that is of interest from an economical point of view. The experimental finding of this work should bring a better mechanical description of hybridized materials that could be implemented for the description of a numeric twin in predictive tools, for modeling under a variety of mechanical loadings.

Thus, UD carbon fiber prepregs of two quality grades were used to investigate their hybridization and anisotropic response. Hybrid and non-hybrid materials were subjected to off-axis tension testing for three different fiber orientations: 15º, 30º, and 45º, using the DIC technique for strain measurements. However, due to the asymmetric nature of one of the materials the ±45° test is not suitable for shear characterization. Therefore, following the work of Pindera [7], [8], the 45º off-axis test was chosen to determine the in-plane shear modulus G_{12}. The reliability of the off-axis test in determining shear strength was assessed by experimentally evaluating the shear strength for all off-axis tests. A theoretical approximation of shear strength was obtained by fitting the experimental off-axis strength data to the Tsai-Hill failure criterion for uniaxial off-axis strength [6].

2. MATERIALS AND METHODS

2.1 Materials

The materials studied in this work are unidirectional carbon fiber-reinforced composites (UD CFRP). Two prepregs of different qualities were used to manufacture the composite laminates, HSC-500-DT102S-40EF and UTS-150-DT120-32F, which will be referred to as HSC and UTS prepregs, respectively. Both epoxy matrix systems used in this study are manufactured by DeltaTech® and have a medium-temperature curing process. DT102S is a thermosetting epoxy, while DT120 is a toughened thermosetting epoxy with high impact strength. The major difference in the quality of the prepregs relies on the fact that the UTS prepreg has a standardized fiber, with well-known mechanical properties, while for the HSC prepreg, the fiber is not standardized, therefore only the minimum potential values of its mechanical properties are given by the manufacturer. This also affects the cost/areal weight of the prepregs. Both prepregs are produced by DeltaTech® and all laminates were manufactured by Belcoavia S.R.L in Romania.

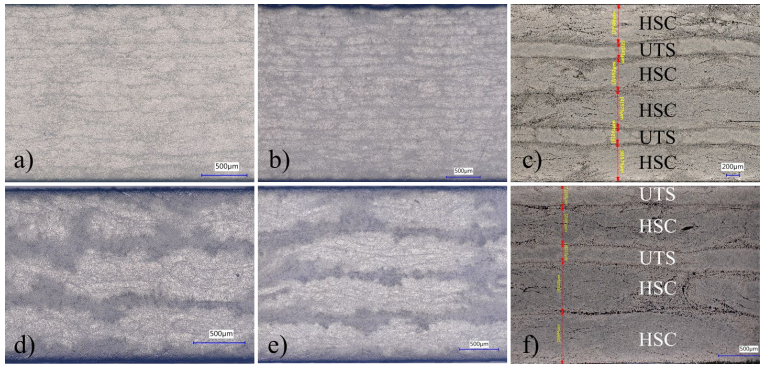

Figure 1. Cross-section views of the materials in this study obtained using a a Keyence VHX-5000 series digital microscope; a) UTS13; b) UTS17; c) H2; d) HSC3; e) HSC4; f) H1

Six laminate types were manufactured, four using a single type of prepreg, while the remaining two employed a combination of HSC and UTS plies to create a ply-level hybrid composite. The hybridization involved variations in ply thickness and material type for the

purpose of cost reduction. Stacking sequences were selected for the hybrid laminates, denoted as H1 and H2, and their areal mass was estimated based on prepreg data. The number of plies for the UTS prepreg laminates was determined to ensure similar areal mass and laminate thickness as H1 and H2 samples. Thus, UTS laminates were produced using 13 and 17 plies, identified as UTS13 and UTS17, respectively. For the HSC prepreg laminates, the number of HSC plies used in each type of hybrid laminate was chosen to manufacture HSC laminates, to determine whether the addition of two UTS plies would result in a difference in mechanical behavior. The HSC laminates were manufactured using 3 and 4 plies, and are referred to as HSC3 and HSC4, respectively. The six laminates are described in Table 1 and cross-sections are shown in Figure 1. The laminate thickness was measured for several samples of each material and the uncertainties are half the range between the maximum and minimum value. All laminate panels were cured in an autoclave, according to the manufacturer's specifications.

Table 1. Laminate details of hybridized and non-hybridized CFRP samples

Name	Stacking sequence	Thickness [mm]	Estimated areal mass [g/m²]	Cost/ fiber areal weight*	Density [g/cm3] [21]	Fiber volume fraction [%][21]
HSC3	$HSC[0°]_3$	1.69±0.02	2499 ± 162	1	1.483 ± 0.005	49.84
HSC4	$HSC[0°]_4$	2.24±0.03	3332 ± 216	1	1.483 ± 0.005	49.31
UTS13	$UTS[0°]_{13}$	2.1±0.05	2860 ± 169	1.4	1.497 ± 0.009	54.46
UTS17	$UTS[0°]_{17}$	2.7±0.04	3740 ± 221	1.6	1.490 ± 0.004	53.67
H1	2HSC+1UTS+1HSC+1UTS[0º]	2.19±0.03	2939 ± 164	1.1	1.478 ± 0.007	50.32
H2	HSC+UTS+2HSC+UTS+HSC [0º]	2.7±0.01	3772 ± 218	1.2	1.499 ± 0.011	52.14

*Normalized to the cost/fiber areal weight of HSC laminates

2.2 Experimental setup

Quasi-static tension tests are performed to determine the off-axis response of the UD laminates for three different fiber orientations: 15º, 30º, and 45º. Guidelines from EN ISO 527-5 [22] standard were followed to conduct these tests. All mechanical tests were carried out at ambient temperature (20° C) and controlled in displacement at 1 mm/min, giving an approximate strain rate of 10^{-4} 1/s. An electromechanical testing machine INSTRON® 5960, with a load cell of 50 kN and wedge grips was used for all tensile tests.

As in our previous study [21], GOM Aramis® 5M was used for DIC measurements, post-processing, and extraction of the strain values. The software package (ARAMIS Version 6.3) is designed to run the GOM sensor and controller, create the project files, process the recorded images, compute results, and perform the post-processing for data extraction.

The GOM ARAMIS 5M sensor consists of two CCD cameras with a resolution of 2448 pixels x 2050 pixels. Lenses with a focal distance of 50 mm and no zoom were used. The calibration of the system was performed using a QCG 2045 32 mm x 24 mm calibration cube and instructions from the user manual. The images were acquired at a speed of 1 image per

second. The tensile force from the tensile machine was imported via the A/D input of the sensor controller for a better correlation of the force and corresponding displacement.

The DIC analysis requires a high-contrast stochastic pattern on the investigated sample. A reference image of the undeformed sample is recorded before the test, and sequential images of the deformed sample are recorded during the tensile test. In the post processing step, an analysis based on tracking the unique surface patterns is made using the ARAMIS V6.3 software, to provide a progressive measurement of surface deformation. For DIC processing, a subset size of 19 x 19 pixels with a step size of 10 pixels, and an overlap area of 9 pixels was used. In standard conditions, the standard deviation for in-plane displacements is up to 0,4 µm, based on the user manual of the system. After calibrating the GOM system, out of the 150 mm of the sample's gauge length, only 75mm were in the field of view of the camera system.

2.3 Sample preparation

Because the materials were provided in two different batches, a year apart, they were cut using methods available at those specific times. Thus, H1 samples were provided first and were cut using a milling machine at the manufacturer's facility, and all other laminates were cut using water-jet cutting at Université de Bretagne Occidentale in Brest, France. In all cases, sample edges were controlled by visual checking so that they did not exhibit any visible asperities that could influence the tests. Aluminum end tabs were used to reduce the gripping effects and were bonded with Araldite 420 A/B Epoxy Adhesive System. For H1, 2 mm thick aluminum tabs were used, while for all other materials, tabs of 1.5 mm in thickness were applied.

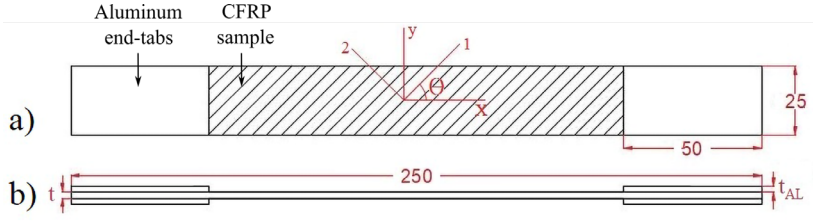

Figure 2. Samples dimensions in mm; a) top view of sample b) side view of sample; t – thickness of the sample, tAL – thickness of aluminum tabs , according to EN ISO 527-5 [22] standard

The speckle pattern for DIC measurement was obtained by first painting the specimen with a matte white spray paint that was applied directly onto the specimen. After drying, matte black spray paint was applied by intended overspray to create a random pattern.

In Figure 2, the nominal dimensions of the samples are presented, with the corresponding axis systems: x – the load direction, y- transverse direction, 1 – fiber direction, 2 – transverse to the fiber direction, and θ – off-axis angle. A minimum of three samples were tested for each configuration, and for H1 material, six samples were tested due to availability of the material at the time of the experimental campaign. For HSC4, the Aramis project file for two 15° tests was corrupted when transferring to a different hard-drive and the project file could not be opened to perform the DIC analysis and retrieve the strain data, therefore data for only one test is available.

3. THEORY AND CALCULATION

3.1 DIC Data processing

DIC data were used for establishing the evolution of stress versus strain. A successive linear regression procedure was employed to select the linear stress-strain data at the origin, from

which the apparent modulus E_x are estimated. The schematic diagram of this method is detailed in Figure 3. The proposed method uses successive least-squares linear regressions. An initial regression is calculated using the first set of experimental points. Thereafter, the next regressions are calculated after adding additional experimental points to the initial dataset. For each regression, the coefficient of determination R^2 is calculated. R^2 is a measurement of the correlation between a fitted model and the experiment data points. A value of 1 is an indication that the regression model fits perfectly the dataset. In the proposed procedure, the number of points from the dataset for which the regression has the maximum R^2 is saved and another potential maximum R^2 is searched in the vicinity, by adding or subtracting one data point. The apparent modulus is extracted as the slope of the linear fit for the stress-strain data points for which the regression had a maximum R^2.

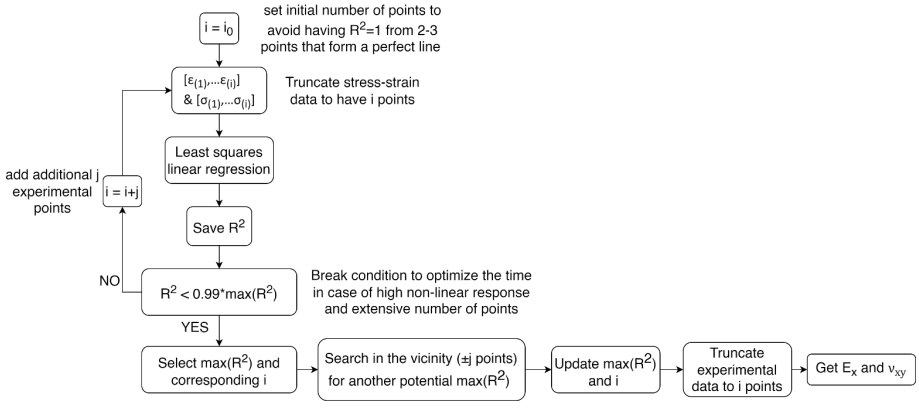

Figure 3. Flowchart of the successive linear regression procedure on stress-strain relations obtained from experimental data extracted with DIC

Before employing the successive linear regression procedure, all stress-strain curves were smoothed using the 'Smooth' function in MATLAB® with the 'Lowess' method to minimize the influence of minor variations in the stress-strain data on the successive linear fits [23]. Furthermore, to avoid any influence of signal noise at the beginning of the tensile test due to grip/sample alignment on the extraction process, the stress-strain data up to a strain value of 5.10^{-4} was not considered.

3.2 Shear characterization

The in-plane shear modulus is evaluated from 15º, 30º, and 45º off-axis tests, for comparison purposes. For calculations in which the in-plane shear modulus is required, the value extracted from the 45º off-axis test is used, based on recommendations of Pindera et al. [7], [8].

The Tsai-Hill failure criterion for uniaxial off-axis strength [6] is used to obtain an approximate shear strength. The Tsai-Hill failure criterion is detailed in equation (1), in which θ is the off-axis angle, X is the failure stress in the fiber direction, Y is the failure stress in the direction perpendicular to the fiber, and S represents the shear failure stress or shear strength. The shear strength S is adjusted so that the failure stress prediction using the Tsai-Hill criterion fits the off-axis experimental data for failure stress.

$$\frac{\cos^4\theta}{X^2}+\left[\frac{1}{S^2}-\frac{1}{X^2}\right]\cos^2\theta\sin^2\theta+\frac{\sin^4\theta}{Y^2}=\frac{1}{\sigma_{xx}^2} \tag{1}$$

The shear stress in a composite ply with fibers oriented at an angle θ relative to the direction of the load can be evaluated by using a coordinate transformation. The simplified

equation (2) can be used in which the end-constraint effects are ignored [7]. The in-plane shear strain can be evaluated based on the structural-axes strains using equation (3) [9].

In equations (1), (2), and (3), the notations are as follows: x and y are the structural directions, with x in the loading direction; 1 and 2 are the axes of the composite coordinate system, with 1 in the fiber direction. The layout of the off-axis specimens and used coordinate systems are detailed in Figure 2.

$$\tau_{12} = -\sigma_{xx} \cdot \cos\theta \cdot \sin\theta \tag{2}$$

$$\gamma_{12} = (\varepsilon_{yy} - \varepsilon_{xx}) \sin 2\theta + \gamma_{xy} \cos 2\theta \tag{3}$$

The in-plane shear modulus G_{12} is determined from the slope of the tangent to the shear stress-shear strain plot, in the linear response region, with the successive linear regression method that was previously described.

3.3 Transverse isotropy

If the composite is transversely isotropic and the in-plane elastic properties are known, the off-axis apparent elastic modulus E_x can be predicted using the transformation equation (4). Thus, based on the in-plane properties previously determined in [21] and the shear modulus estimated in this work, a comparison of the experimental and theoretical apparent modulus is performed.

$$\frac{1}{E_x} = \frac{1}{E_1}\cos^4\theta + \left[\frac{1}{G_{12}} - \frac{2\nu_{12}}{E_1}\right]\sin^2\theta\cos^2\theta + \frac{1}{E_2}\sin^4\theta \tag{4}$$

4. RESULTS AND DISCUSSIONS

4.1 Off-axis response

All testing configurations achieved good repeatability, with at least three tested samples, allowing the selection of representative tests for visualization and qualitative comparisons. For all tensile tests, no sliding was observed within the end-tabs during tensile testing.

4.1.1 15° off-axis test

Figure 4 illustrates stress-strain responses from 15° off-axis tests. All laminates demonstrate a prominent non-linear stress-strain behavior, with the onset of non-linearity occurring around 110-120 MPa. Notably, the thickness of HSC3 and HSC4 laminates (1.69 mm and 2.24 mm, respectively) does not seem to influence their stress-strain response (Figure 4a). Conversely, UTS13 and UTS17 laminates, with respective thicknesses of 2.10 mm and 2.70 mm, exhibit a slight disparity in stress levels within the non-linear range (Figure 4b), indicating strain hardening in UTS17 compared to UTS13. Although void content could potentially affect the strain hardening behavior by promoting localized deformation and internal failure, the similarity in fiber and void content between UTS13 and UTS17 laminates [20] suggests that these properties do not account for the observed difference in strain hardening. The influence of laminate thickness on strain hardening behavior could be attributed to the potential for fiber-dominated deformation mechanisms in thicker laminates, such as fiber sliding and reorientation, which enhance strain hardening. However, this effect is not observed in the HSC thin-thick laminate pair. Among the hybrid laminates, the thicker laminate H2 exhibits less strain hardening compared to H1 (Figure 4c), indicating that laminate thickness may not play

a significant role in strain hardening for the tested laminates. The difference in strain hardening response between the hybrid laminates could be attributed, among other factors, to variations in void content. Although the average void content is under 1%, the void content of H2 is twelve times higher than that of H1 [20]. Figure 4d presents a comparison of the stress-strain response under 15° off-axis tensile loading using representative tests for each material configuration. While differences in the linear response regime are negligible, HSC laminates exhibit greater strain hardening and lower failure strain compared to UTS laminates. Both hybrid laminates reach higher stress levels than the simple laminates and demonstrate intermediate failure strain. These distinct behaviors cannot be solely attributed to void content, as H2 and UTS laminates have similar void content, indicating that ply-level hybridization induces a strain-hardening effect.

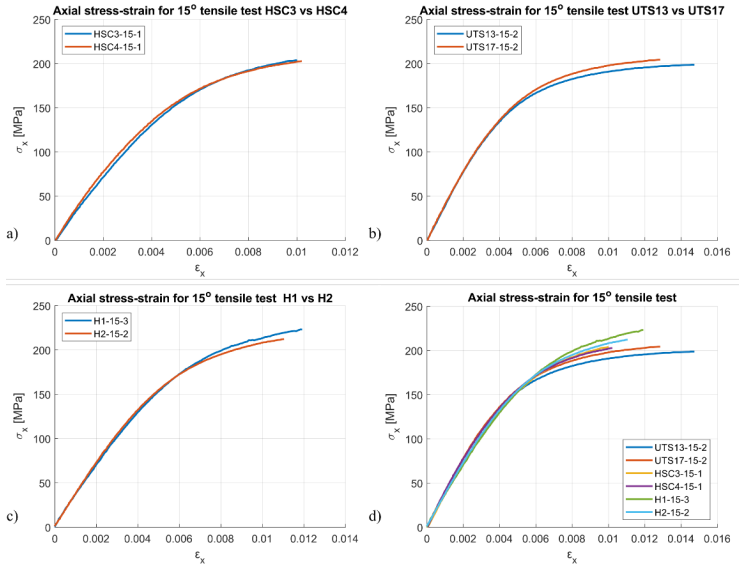

Figure 4. Comparison of axial stress-strain response under 15° off-axis tensile test for representative samples of each laminate configuration; at 1 mm/min, from DIC analysis, a) HSC3 vs HSC4; b) UTS13 vs UTS17; c) H1vs H2; d) Simple and hybrid configuration materials

Table 2 provides the average values of the apparent Young's modulus, failure stress, and failure strain for all laminates, with uncertainties represented by half the measurement range. Notably, there are discrepancies of up to 6 GPa among the average values of the apparent modulus for different configurations. As expected, the UTS laminates exhibit the highest apparent modulus, given their highest in-plane modulus E_{11} among all tested laminates [21]. This is due to the inherently higher elastic modulus of UTS carbon fibers compared to HSC fibers. Additionally, Wang [24] demonstrated that the fiber volume fraction influences the elastic modulus of UD composites. Therefore, variations in the elastic modulus can be attributed to the differences in fiber volume fraction presented in Table 1. While it was anticipated for HSC laminates to have the lowest apparent modulus, considering their lowest in-plane modulus E_{11} and fiber content [21], no clear trend is observed for HSC and hybrid laminates. H1 exhibits the lowest average apparent modulus, while H2 falls between the apparent modulus values of HSC3 and HSC4. The lower apparent modulus in hybrid laminates could be attributed to a weaker interfacial bond between different plies, as a strong bond enhances load transfer and contributes to a higher apparent modulus, while a weak or incompatible interface can lead to stress concentration and reduced stiffness. Although the

matrix system compatibility is not expected to be an issue, as the manufacturer states their compatibility for curing together, further investigations are necessary to evaluate the bond quality of the plies.

Table 2. Experimental results 15° off-axis tensile testing at 1 mm/min, deduced from DIC analysis.

Material	UTS13	UTS17	HSC3	HSC4	H1	H2
E_x $[GPa]$	39± 2	40 ± 2	36± 2	39	34 ± 3	38 ± 2
Failure Stress σ_x [MPa]	199 ± 1	200 ± 11	204 ± 2	203	218 ± 12	212.2 ± 0.5
Failure strain ε_x	0.015 ± 0.001	0.012 ± 0.002	0.0100 ± 0.0002	0.010 2	0.011 ± 0.002	0.0106± 0.0005

Regarding the failure stress and failure strain, the UTS laminates exhibit the lowest average failure stress and the highest failure strain, which is reflected in the stress-strain behavior as an almost plateau response before failure. These laminates also show the most pronounced non-linear behavior of all. As previously mentioned, UTS17 demonstrates strain hardening in comparison to UTS13, with a similar average failure stress but a wider range of measurements, potentially indicating higher failure stress. UTS13 exhibits a 16% higher failure strain (including uncertainties). For HSC laminates, no significant difference is observed between HSC3 and HSC4. Compared to UTS laminates, HSC laminates show a slight increase in failure stress (approximately 2%) but a significant decrease in failure strain (approximately 32% compared to UTS13). Among hybrid laminates, H1 has a higher average failure stress than H2 (around 3% increase), but with higher uncertainty due to a larger number of tested H1 samples, which may lead to premature failure due to local material defects. Further analysis is needed to establish an appropriate criterion for assessing failure stress in H1 compared to H2. Nevertheless, even when considering the lowest failure stress values, both hybrid configurations exhibit higher failure stress than UTS and HSC laminates. In terms of average failure stress, H1 shows a 9% increase compared to UTS laminates and a 6% increase compared to HSC laminates, while H2 has a lower percentage increase (6% compared to UTS laminates and 4% compared to HSC laminates). Regarding average failure strain, the hybrid laminates fall between the reference laminates, with an approximately 8% increase between H1 and HSC4, a 4% increase between H2 and HSC4, and a decrease of 26% and 29% between UTS13 and H1 and H2, respectively.

4.1.2 30° off-axis test

As for the 15° off-axis tensile test, a high non-linear stress-strain response is observed in for all laminates during the 30° off-axis test, with the non-linear regime starting at a stress level of 50-60 MPa, which is half of the stress level observed in the 15° off-axis tensile test. No apparent thickness effect was observed for laminates made from the same material.

A comparison of the stress-strain response under 30° off-axis tensile loading using representative tests for each material can be seen in Figure 6. The response in the linear regime is similar across all laminates, while in the non-linear regime, UTS laminates exhibit a more pronounced non-linear response than HSC laminates and hybrid configurations. Similar to the 15° off-axis test, hybrid laminates demonstrate strain hardening compared to reference laminates, reaching higher stress levels at the same strain value.

Table 3 shows the average values of the extracted apparent Young's modulus, failure stress, and failure strain for all laminates during the 30° off-axis test, with uncertainties as half the range of measurements. Differences between the average values of the apparent modulus

of all material configurations do not exceed 1.5 GPa, representing a 10% increase in the apparent elastic modulus for H2 (having the highest average apparent modulus) compared to HSC3 (lowest average apparent modulus).

Table 3. Experimental results 30° off-axis tensile testing at 1 mm/min deduced from DIC analysis.

Material	UTS13	UTS17	HSC3	HSC4	H1	H2
E_x $[GPa]$	15.3± 0.2	15.1 ± 0.5	14± 0.5	14.8± 0.4	15 ± 1	15.4 ± 0.1
Failure Stress σ_x [MPa]	101 ± 2	99 ± 4	104 ± 2	103 ± 1	106 ± 6	105 ±2
Failure strain ε_x	0.019 ± 0.003	0.015 ± 0.003	0.0140 ± 0.001	0.013± 0.003	0.012 ± 0.002	0.010± 0.004

For averaging the failure stress and strain, samples that failed prematurely compared to were not taken into account. As for the 15° off-axis tensile test, the UTS laminates have the lowest failure stress and the highest failure strain. HSC laminates have a higher failure stress and lower strain compared to UTS laminates but when looking at the hybrid configurations, they have the highest failure stress and lowest failure strain. There is no significant difference between HSC3 and HSC4, and compared to UTS laminates, HSC laminates have a higher failure stress with a percentage increase of approximately 2%. However, a percentage decrease of approximately 32% was found between UTS13 (this laminate was chosen for reference as it has the highest failure strain) and HSC laminates in terms of failure strain.

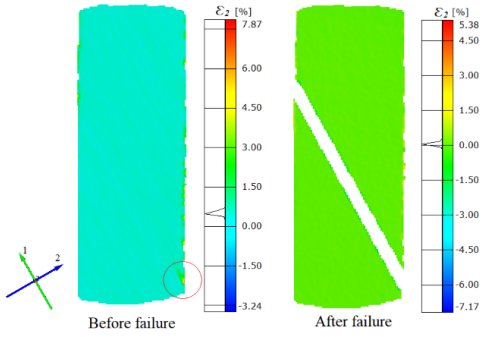

Figure 5. Transverse strain field ε_2 deduced from the Digital Image Correlation for H1-30-3 sample, under 30 off-axis tensile tests; before failure (left) and after failure (right)

By analyzing the strain distribution in the matrix direction 2 in Figure 5, computed by rotating the original coordinate system at 30°, it can be observed by DIC that at the edge of the sample, marked with a red circle, there is a strain in the matrix of 7.87% compared to a strain of less than 1.5% in the rest of the sample. Comparing the position of the strain concentration with the position of the failure in the other image, it was concluded that failure started from the edge of the sample, with a matrix failure due to the high strain in the region. It may be assumed that for the other samples, including for other off-axis angles, the failure started in a similar manner. This finding is consistent with the work of Hu et al. [14], where strain field analysis using DIC for the 45° specimens revealed the highest strain occurring at the corner of the sample's edge.

4.1.3 45° off-axis test

Representative tests at 45° off-axis were selected for each material and comparisons are illustrated in Figure 6. All material systems displayed a non-linear regime beginning at around

30-40 MPa stress level, although this effect was less pronounced compared to the stress-strain response for 15° and 30° off-axis angles. There was no apparent thickness effect observed for UTS laminates and HSC laminates. The same strain hardening for the hybrid laminates compared to the reference ones can be observed. Although the difference in the value of the stress is not as high as for previously analyzed off-axis angles, the percentage increase in stress level is still around 10%.

Table 5 provides the average values of the apparent Young's modulus, failure stress, and failure strain for all laminates, with uncertainties as half the range of measurements. The differences between the average values of the apparent modulus for all material configurations were very small, with less than a 0.5 GPa difference. H2 had the highest apparent modulus, while HSC3 had the lowest, with a percentage increase of approximately 3% instead of 10%.

Table 4. Experimental results 45° off-axis tensile testing at 1 mm/min from DIC.

Material	UTS13	UTS17	HSC3	HSC4	H1	H2
E_x $[GPa]$	9.3± 0.1	9.3 ± 0.5	9.1± 0.2	9.1± 0.1	9.2 ± 0.2	9.4 ± 0.4
Failure Stress σ_x [MPa]	70 ± 3	72 ± 2	67 ± 4	69± 5	60 ± 12	67 ±2
Failure strain ε_x	0.012 ± 0.002	0.013 ± 0.001	0.010 ± 0.001	0.011± 0.002	0.008 ± 0.002	0.009± 0.001

The differences in failure stress and failure strain are more noticeable, with UTS laminates displaying the highest values and both hybrid laminates having the lowest average failure stress and lowest failure strain. Although H1 and H2 reach higher stress levels compared to HSC and UTS laminates for the same strain value in the non-linear response regime, the failure stress is also the lowest due to a very low failure strain. Additionally, 45° off-axis samples were more prone to fail near the grips than 15° and 30° off-axis samples, which could also influence the values of failure parameters.

4.2 Stress to fiber orientation response

Since the stress-strain response of each specimen in the same test configuration fluctuated slightly, for the sake of comparison of the results for various off-axis angles, only one specimen in each loading condition was selected as representative, for a qualitative comparison, shown in Figure 6. The on-axis stress-strain response is taken from our previous work [21] and the response for the 0° test was truncated to have a clearer view of the response at the other angles.

With decreasing off-axis angle, each material exhibits a higher degree of non-linear response, which aligns with findings reported by Zhao et al. [25]. Additionally, there is an evident decrease in the apparent elastic modulus as the off-axis angle increases. Moreover, across all off-axis angles, the hybrid materials demonstrate higher stress levels at the same strain value compared to materials composed solely of UTS or HSC plies within the non-linear response region. Furthermore, the disparity in stress levels between the materials becomes more pronounced with increasing non-linearity in the stress-strain response. This effect is particularly noticeable in the 15° tensile test compared to the 45° tensile test.

The results of the apparent axial elastic moduli E_x obtained from each off-axis angle are summarized in Figure 7, using the average value for each test configuration. A significant difference in the apparent elastic modulus can be observed depending on the off-axis angle. Compared to the elastic modulus at 0° orientation, the apparent modulus at 45° and 90° is only 7.3-8% and 5.5-6.3% respectively. The percentage interval is calculated based on the individual percentage for each material configuration. The measured moduli were compared with the prediction based on the transformation relation in equation (4), using the elastic

properties along the principal material direction. The prediction aligns well with the experimental results for all material configurations, with an overestimation of less than 12% in the worst case. Hence, both the reference materials and the ply-level hybrid carbon composite materials can be modeled as transversely isotropic systems.

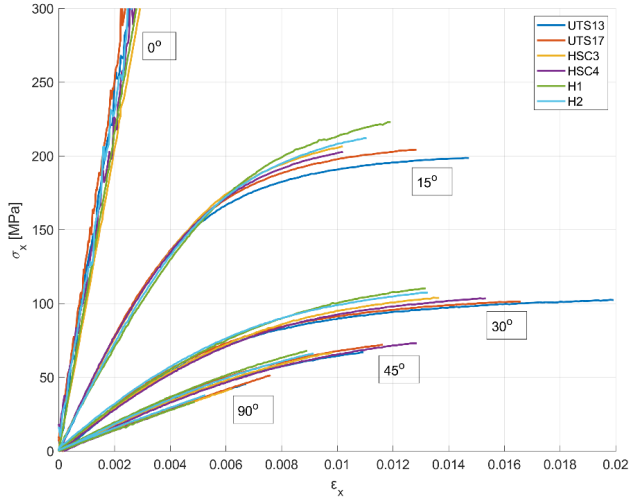

Figure 6. Stress-strain curves obtained by DIC of on and off-axis specimens at 1 mm/min

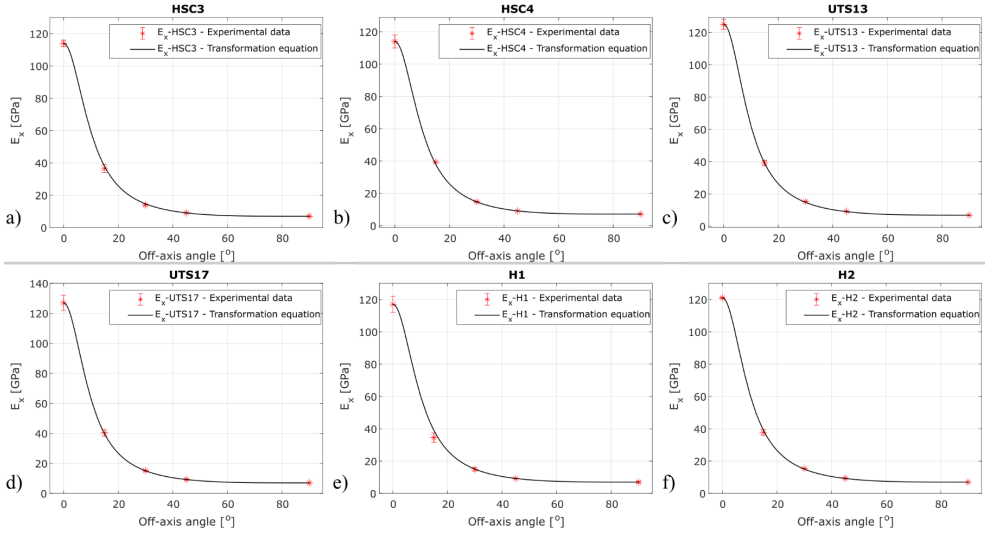

Figure 7. Comparison of the apparent Young's modulus deduced from DIC (crosses) and calculated by the transformation relation (4) for various off-axis angles; a) HSC3; b) HSC4; c) UTS13; d) UTS17; e) H1; f) H2

Regarding the failure stress, a significant reduction with increasing off-axis can be observed in Figure 6 but the drop is illustrated better in Figure 8 in which the averaged axial strength and strain for each test configuration are presented. The same trend was observed for all laminate configurations. A sharp decline was observed when the off-axis angle increased from 0° to 15°, with a decrease in strength around 86-89%, depending on the material. Between the following consecutive off-axis angles, the decrease is not as significant as the first one, with 51-55% from 15° to 30°, 27-43% from 30° to 45° and 36-53% from 45° to 90°, but still, the lowest strength, for θ=90°, represents only 1.8-3% of the strength in 0°.

Predictions of the failure stress were also made using the Tsai-Hill failure criterion for uniaxial off-axis strength, detailed in equation (1). The predictions agree well with the experimental data for the adjusted shear strength *S* of each material configuration. The *S* values used for fitting the Tsai-Hill failure criterion to the experimental data are mentioned in the figure's caption.

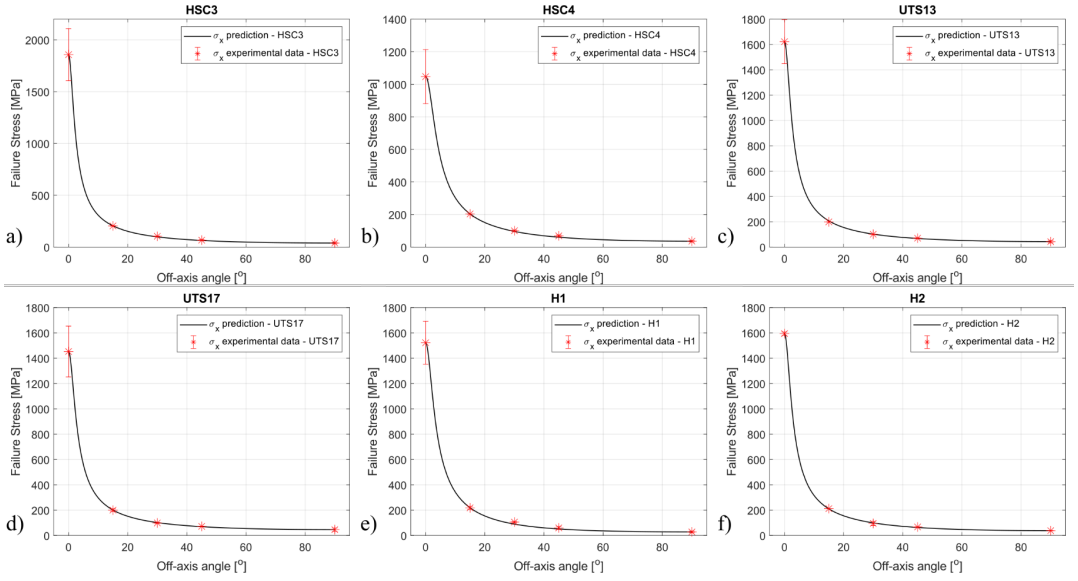

Figure 8. Failure stress at various off-axis angles, with predictions using Tsai-Hill criterion; a) HSC3 - S=55 MPa; b) HSC4 - S=56 MPa; c) UTS13 - S=55 MPa; d) UTS17 - S=53 MPa; e) H1 - S=65 MPa; f) H2 - S=57 MPa

4.3 In-plane shear properties results

Off-axis tensile test results were utilized to extract the shear stress-strain response and shear modulus, as outlined in section 3. The calculated shear strain γ_{12} based on equation (3), extracted from the 45° off-axis test was also compared with the shear strain extracted directly from the GOM Aramis® software after rotating the coordinate system with 45°, and a minor difference between the two was observed. Thus, the shear strain calculated with equation (3) was further used, regardless of the off-axis angle.

For the coordinate system used, shear strain values are negative. In all plots, the absolute values of the shear strain are used. As both shear stress τ_{12} and shear strain γ_{12} are extracted from axial stress and strain using coordinate transformation equations, the shear stress-shear strain curves for the tested samples of all materials have the same good reproducibility as for the off-axis tensile test from which they were extracted. They also share the non-linear stress-strain response.

The same observations made for the axial stress-strain response of corresponding tests are applicable. In all cases, the hybrid laminates present a strain hardening in the nonlinear response regime, which leads to higher shear stress levels at the same strain values compared to reference materials.

The average values of the in-plane shear modulus extracted from all off-axis test types are given in Table 5, with uncertainties as half the range of measurements. It can be observed that for all materials, except H1, the shear modulus extracted from 15° and 30° are higher than the ones extracted from the 45° off-axis test.

A similar observation was also made by [7], but with a higher difference in the values of the shear modulus extracted from different off-axis angles tests, and they concluded that the 45° off-axis test is the most reliable in estimating the in-plane shear modulus, as the effects of end-constraints are minimized compared to other angles. For further calculations, the modulus extracted from the 45° off-axis test will be used.

Table 5. Shear modulus G_{12} values from off-axis tensile testing

Material	UTS13	UTS17	HSC3	HSC4	H1	H2
G_{12} from 45° [GPa]	3.42± 0.04	3.48 ± 0.22	3.40± 0.05	3.38± 0.02	3.49 ± 0.04	3.48 ± 0.17
G_{12} from 30° [GPa]	3.56± 0.01	3.49 ± 0.07	3.22± 0.12	3.42± 0.09	3.46± 0.21	3.56 ± 0.02
G_{12} from 15° [GPa]	3.74 ± 0.64	3.64± 0.20	3.64 ± 0.10	3.8	3.32 ±0.95	3.50 ±0.23
Shear failure stress τ_{12} from 45° [MPa]	35 ± 2	36 ± 1	33 ± 2	34 ± 3	30 ± 6	33 ± 1
Shear failure stress τ_{12} from 30° [MPa]	43.9± 0.7	43 ± 2	45± 0.7	43± 2.2	46 ± 3	41 ± 7
Shear failure stress τ_{12} from 15° [MPa]	49.8 ± 0.3	50± 3	51 ± 0.6	50.7	54 ±3	53.1 ±0.1
Shear failure stress estimation using Tsai-Hill failure criterion* [MPa]	55	53	55	56	65	57

**S* parameter that was adjusted to fit Tsai-Hill failure criterion to off-axis failure stress experimental data.

Average values of shear failure stress and the values used as the shear strength parameter S in Tsai-Hill failure criteria (section 4.2) are provided in Table 5. The shear stress extracted from the 15° off-axis tensile test surpasses that from the 30° or 45° tests, indicating significant variation. Furthermore, for all materials, the experimental shear failure stress from off-axis tensile tests falls below the shear strength value that aligns with the axial failure stress prediction using Tsai-Hill failure criteria. This implies that the shear failure stress from off-axis tensile tests ($\theta \geq 15°$) is underestimated and cannot be considered reliable.

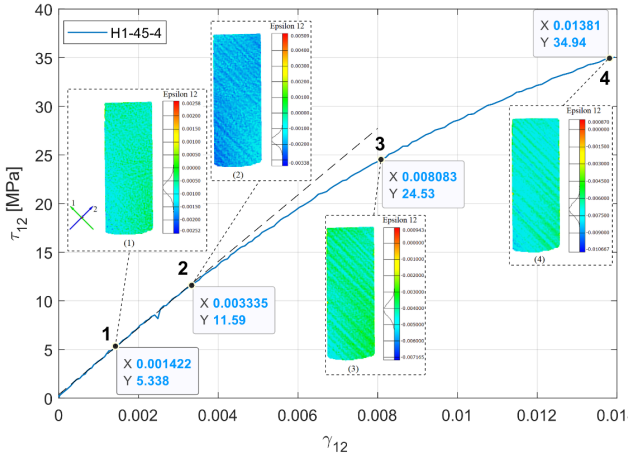

Figure 9. In-plane shear stress-strain response with corresponding points for DIC full-field analysis; tensile test on H1-45-4 sample at 1 mm/min. Color maps show in-plane ε_{12} full-field distribution from Digital Image Correlation analysis, at different time steps during 45° off-axis test

Figure 9 presents a full-field analysis of the shear strain distribution for a H1 material sample subjected to a 45° off-axis test, focusing on specific points selected from the shear stress-strain curve. Given the non-linear nature of the in-plane shear response, four points were chosen for the analysis, as highlighted in Figure 9. These points include the first one in the linear response region, the second point near the onset of the non-linear region, the third point at a higher shear strain within the non-linear response region, and the fourth point near failure. Furthermore, the original coordinate system (with x representing the loading direction and y perpendicular to it) was rotated by 45°. Thus, the color maps in the coordinate system reflect the material's principal direction, with 1 representing the fiber direction and 2 - perpendicular to it. When comparing shear values in Figure 9, it should be noted that the color maps represent the tensorial strain ε_{12} (extracted from GOM Aramis® software), which is half the engineering shear γ_{12} used in shear stress-strain plots. The in-plane shear distribution on the sample's surface shows an uneven shear distribution at point 1, lacking a clear contour, while the other 3 points exhibit visible shear strain distribution aligned with the 45° angle of the fibers. Near the failure point, the fourth image reveals shear concentration at the sample's edges, suggesting failure initiation and propagation from the edges. Additionally, the presence of higher shear lines can be attributed to increased shear in the fiber-bonding matrix.

5. CONCLUSIONS

This study aimed to evaluate hybridized composite materials' mechanical performance compared to high-standard reference materials for cost-effective structural applications in the aerospace industry. A ply-level-hybridization approach was used to create laminates with varying ply thicknesses and material qualities by combining two types of carbon fiber prepregs. Monotonic quasi-static off-axis tests were performed to assess the off-axis behavior, with Digital Image Correlation used for strain analysis. The results showed non-linear stress-strain behavior, with decreased nonlinearity at higher off-axis angles. Hybrid laminates exhibited strain hardening and higher failure stress levels compared to simple laminates. Thickness effects were minimal in the linear response region but slight differences in stress levels were noted for laminates with the same material but different thicknesses in the non-linear response region. Off-axis elastic moduli and strength degraded with increasing off-axis angles. The hybridization approach demonstrated benefits in terms of strain hardening and failure stress. Additionally, the hybrid laminates demonstrated behavior resembling that of a transversely isotropic system. However, further analysis is required to fully understand the mechanism behind the enhanced non-linear response and strain hardening behavior.

ACKNOWLEDGMENTS

The first author acknowledges the financial support of Campus France for internships at ENSTA Bretagne, where the experimental tests were conducted. The authors also express gratitude to Belcoavia S.R.L. for manufacturing the composite plates, Thomas Bonnemains from IUT Brest for water-jet cutting of the samples, and the staff at ENSTA Bretagne, particularly Claudiu Bădulescu, for their guidance and assistance with the experimental equipment.

REFERENCES

[1] A. M. Pawlak, T. Górny, Ł. Dopierała, and P. Paczos, The Use of CFRP for Structural Reinforcement - Literature Review, *Metals*, vol. **12**, no. 9, p. 1470, 2022, doi: 10.3390/MET12091470.

[2] P. T. Curtis and M. Browne, Cost-effective high performance composites, *Composites*, vol. **25**, no. 4, pp. 273–280, 1994, doi: 10.1016/0010-4361(94)90219-4.
[3] C. Audibert, A. S. Andreani, É. Lainé, and J. C. Grandidier, Mechanical characterization and damage mechanism of a new flax-Kevlar hybrid/epoxy composite, *Composite Structures*, vol. **195**, pp. 126–135, 2018, doi: 10.1016/J.COMPSTRUCT.2018.04.061.
[4] P. Zuo, D. V. Srinivasan, and A. P. Vassilopoulos, Review of hybrid composites fatigue, *Composite Structures*, vol. **274**, p. 114358, 2021, doi: 10.1016/J.COMPSTRUCT.2021.114358.
[5] D. Gay, *Composite materials : design and applications*, Third Edit. Boca Raton: CRC Press, 2015.
[6] R. M. Jones, *Mechanics Of Composite Materials*, 2nd ed. New York: Taylor & Francis, 1999. doi: 10.1201/9781498711067.
[7] M. J. Pindera and C. T. Herakovich, Shear characterization of unidirectional composites with the off-axis tension test, *Experimental Mechanics*, vol. **26**, no. 1, pp. 103–112, 1986, doi: 10.1007/BF02319962.
[8] M. J. Pindera, G. Choksi, J. S. Hidde, and C. T. Herakovich, A Methodology for Accurate Shear Characterization of Unidirectional Composites, *Journal of Composite Materials*, vol. **21**, no. 12, pp. 1164–1184, 1987, doi: 10.1177/002199838702101205.
[9] C. C. Chamis and J. H. Sinclair, Ten-deg Off-axis Test for Shear Properties in Fiber Composites, *Experimental Mechanics*, vol. **17**, pp. 339–346, 1977.
[10] G. Vargas and F. Mujika, Determination of In-plane Shear Strength of Unidirectional Composite Materials Using the Off-axis Three-point Flexure and Off-axis Tensile Tests, *Journal of Composite Materials*, vol. **44**, no. 21, pp. 2487–2507, 2010, doi: 10.1177/0021998310369601.
[11] H. T. Hahn and S. W. Tsai, Nonlinear Elastic Behavior of Unidirectional Composite Laminae, *Journal of Composite Materials*, vol. **7**, no. 1, pp. 102–118, 1973, doi: 10.1177/002199837300700108.
[12] S. Ogihara, Nonlinear Mechanical Response of CFRP Laminates under Off-Axis Tensile Loading, *Science and Engineering of Composite Materials*, vol. **17**, no. 2, pp. 133–141, 2010, doi: 10.1515/SECM.2010.17.2.133.
[13] D. Cai, G. Zhou, X. Wang, C. Li, and J. Deng, Experimental investigation on mechanical properties of unidirectional and woven fabric glass/epoxy composites under off-axis tensile loading, *Polymer Testing*, vol. **58**, pp. 142–152, 2017, doi: 10.1016/J.POLYMERTESTING.2016.12.023.
[14] Y. Ma, Y. Li, and L. Liu, Off-Axis Tension Behaviour of Unidirectional PEEK/AS4 Thermoplastic Composites, *Applied Sciences*, vol. **13**, no. 6, p. 3476, 2023, doi: 10.3390/APP13063476.
[15] * * * ASTM International, ASTM D4255/D4255M-15a Standard Test Method for In-Plane Shear Properties of Polymer Matrix Composite Materials by the Rail Shear Method, 2020.
[16] * * * ASTM International, ASTM D5379/D5379M - Standard Test Method for Shear Properties of Composite Materials by the V-Notched Beam Method, 2019.
[17] S. Yoon Park and W. Jong Choi, Review of material test standardization status for the material qualification of laminated thermosetting composite structures, *Journal of Reinforced Plastics and Composites*, vol. **40**, no. 5–6, pp. 235–258, 2020, doi: 10.1177/0731684420958107.
[18] * * * ASTM International, ASTM D3518/D3518M - Standard Test Method for In-Plane Shear Response of Polymer Matrix Composite Materials by Tensile Test of a ±45° Laminate, 2018
[19] M. Merzkirch and T. Foecke, 10° off-axis testing of CFRP using DIC: A study on strength, strain and modulus, *Composites Part B: Engineering*, vol. **196**, p. 108062, 2020, doi: 10.1016/j.compositesb.2020.108062.
[20] C. Goidescu, H. Welemane, C. Garnier, M. Fazzini, R. Brault, E. Péronnet, and S. Mistou, Damage investigation in CFRP composites using full-field measurement techniques: combination of digital image stereo-correlation, infrared thermography and X-ray tomography, *Composites Part B: Engineering*, vol. **48**, pp. 95–105, 2013, doi: 10.1016/J.COMPOSITESB.2012.11.016.
[21] M. Casapu, I. Fuiorea, and M. Arrigoni, Experimental Characterization of Internal Structure and Physical Properties of Unidirectional Ply-Level Hybrid Carbon Composite Material, *Advanced Engineering Materials*, 2023, doi: 10.1002/ADEM.202201447.
[22] * * * British Standards Institution, BS EN ISO 527-5:2009: Plastics. Determination of tensile properties. Test conditions for unidirectional fibre-reinforced plastic composites, 2009
[23] * * * MATLAB, *version 9.8.0.1417392 (R2020a)*. Natick, Massachusetts: The MathWorks Inc., 2020.
[24] H. W. Wang, H. W. Zhou, L. L. Gui, H. W. Ji, and X. C. Zhang, Analysis of effect of fiber orientation on Young's modulus for unidirectional fiber reinforced composites, *Composites Part B: Engineering*, vol. **56**, pp. 733–739, 2014, doi: 10.1016/J.COMPOSITESB.2013.09.020.
[25] Y. Q. Zhao, Y. Zhou, Z. M. Huang, and R. C. Batra, Experimental and micromechanical investigation of T300/7901 unidirectional composite strength, *Polymer Composites*, vol. **40**, no. 7, pp. 2639–2652, 2019, doi: 10.1002/PC.25059.